AIAA JOURNAL
Vol. 33, No. 11, November 1995

Evaluation of Boundary Conditions for Computational Aeroacoustics

R. Hixon,* S.-H. Shih,* and Reda R. Mankbadi†
NASA Lewis Research Center, Cleveland, Ohio 44135

The performance of three acoustic boundary condition formulations is investigated by computing a test problem with a known analytic solution. By using a fixed grid and time step, all variations in the solution are due solely to the boundary condition. The effect of implementation differences on the performance of a given boundary condition is also studied. Details of all implementations are given. Results are shown for the acoustic field of a monopole in a uniform freestream.

Nomenclature

A, B, C	= coefficient matrices (nonconservative equations)
$\bar{c}$	= mean speed of sound
c_1, c_2, c_3, c_4	= radial one-dimensional characteristic variables (Giles)
E	= mean energy
$\tilde{F}, \tilde{G}, \tilde{H}$	= perturbation flux vectors
k, l	= axial and radial wave number
L_x, L_r	= numerical operators
L_1, L_2, L_3, L_4	= amplitude of one-dimensional characteristic waves (Thompson)
M	= mean Mach number
p'	= perturbation pressure
Q	= vector of flow properties (nonconservative equations)
$\tilde{Q}$	= vector of conserved perturbation quantities
r_1, r_2, r_3, r_4	= axial one-dimensional characteristic variables (Giles)
r_i, l_i	= right and left one-dimensional eigenvectors (Thompson)
S	= similarity transform matrix (Thompson)
$\hat{S}$	= monopole source strength
$\tilde{S}$	= perturbation source term
U, V	= mean axial and radial velocities
γ	= ratio of specific heats
Λ	= matrix of eigenvalues (Thompson)
λ_i	= one-dimensional eigenvalues (Thompson)
$\bar{\rho}$	= mean density
$\rho', (\rho u)', (\rho v)', (\rho e)'$	= conserved perturbation quantities
ω	= monopole frequency

Subscripts

r	= radial operator
t	= temporal operator
x	= axial operator

I. Introduction

ACCURATE prediction of flow fluctuations representing sound is the goal of computational aeroacoustics (CAA) (see, for instance, Ref. 1). To do this, a grid is constructed that covers the region of interest, and the discretized governing equations are solved on this grid. However, the computational domain is usually finite, and boundary conditions must be imposed at the edges of the grid. These boundary conditions can generate spurious fluctuations that render the computed solution entirely unacceptable.

Most of the classical boundary treatments used in computational fluid dynamics are concerned only with obtaining the mean-flow solution. Several suggestions for boundary conditions for unsteady flows have recently been proposed. These proposals can be classified in three categories: 1) quasi-one-dimensional characteristics,[2,3] 2) decomposition of the solution into Fourier modes,[4] and 3) asymptotic analysis of the governing equations for large distances.[5–8]

The present work is concerned with evaluating these types of boundary conditions by comparing the numerical results obtained with various boundary conditions to a known analytical solution. To accomplish this, a large number of grid points were used to avoid inaccuracies arising from the interior scheme. The effect of implementation of each boundary condition on its performance is also investigated.

II. Governing Equations

The equations that are solved are the axisymmetric linearized Euler equations in conservation form, which are written in cylindrical coordinates as

$$\frac{\partial \tilde{Q}}{\partial t} + \frac{\partial \tilde{F}}{\partial x} + \frac{1}{r}\frac{\partial (r\tilde{G})}{\partial r} = \frac{1}{r}\tilde{S} \tag{1}$$

where

$$p' = (\gamma - 1)\left\{(\rho e)' - [(\rho u)'U + (\rho u)'V] + \tfrac{1}{2}\rho'(U^2 + V^2)\right\} \tag{2}$$

III. Numerical Scheme

The code is a modified split MacCormack solver, which is second-order accurate in time and fourth-order accurate in space. This extension of the MacCormack scheme is known as the 2–4 scheme and was developed by Gottlieb and Turkel.[9] This scheme has been used successfully before by Farouk et al.[10] and Ragab and Sheen[11] for studying nonlinear instability problems in plane shear layers. Sankar et al.[12] have evaluated this scheme for aeroacoustics applications. The solution procedure is as follows.

Equation (1) may be rewritten in operator form as

$$\tilde{Q}^{n+1} = L_{rx}\tilde{Q}^n \tag{3}$$

In words, given the flow variables Q at a time level n, the code computes derivatives in both the radial and axial directions and uses these quantities to advance the flowfield one time step, to the $n + 1$ time level.

In the present code, the operator is split into separate radial and axial contributions:

$$\tilde{Q}^{n+1} = L_r L_x \tilde{Q}^n \tag{4}$$

Received June 15, 1994; revision received Jan. 25, 1995; accepted for publication Jan. 27, 1995.

*Senior Research Associate, Institute for Computational Mechanics in Propulsion. Member AIAA.

†Senior Scientist and Leader, Computational Aeroacoustics. Associate Fellow AIAA.

The operators are applied in a symmetric way to avoid any numerical biasing of the solution:

$$\tilde{Q}^{n+2} = L_x L_r L_r L_x \tilde{Q}^n \tag{5}$$

Each operator consists of a predictor and a corrector step. Each step uses one-sided differencing; for example,

Predictor:

$$\tilde{Q}^{n+\frac{1}{2}} = \tilde{Q}^n - \frac{\Delta t}{6\Delta x}(7F_i - 8F_{i-1} + F_{i-2})^n \tag{6}$$

Corrector:

$$\tilde{Q}^{n+1} = \frac{1}{2}\left[\tilde{Q}^n + \tilde{Q}^{n+\frac{1}{2}} + \frac{\Delta t}{6\Delta x}(7F_i - 8F_{i+1} + F_{i+2})^{n+\frac{1}{2}}\right] \tag{7}$$

To avoid biasing, the sweep directions are reversed between each application of the operators.

Note that two points from outside the domain are required for each sweep. The values of the fluxes at these points are computed using third-order extrapolation.

IV. Mathematical Formulation of Boundary Conditions

The primary objective in CAA is to accurately compute the oscillatory flowfield. Since the computational domain is finite, numerical boundary conditions must be imposed at the grid boundaries. Improper specification of these boundary conditions results in artificial disturbances that can render the computed oscillatory flow solution unacceptable. This problem is most pronounced at subsonic outflows. As such, outflow boundary conditions for subsonic flows have received special attention and will be discussed herein.

A. Thompson's Approach

Thompson[2,3] describes how to decompose hyperbolic equations into wave modes of definite velocity and then how to specify boundary conditions for the incoming waves. The starting point of Thompson's analysis is the nonlinear Euler equations. The essence of his approach is that a one-dimensional characteristic analysis can be performed by considering the transverse terms as a constant source term. The one-dimensional characteristic analysis makes clear which waves are propagating into and out of the computational domain. The amplitude of the outward propagating waves are defined entirely from the variables inside the computational domain, whereas the amplitude of the inward propagating waves are specified as boundary conditions. For nonreflective boundary conditions, the amplitudes of the inward propagating waves are set to zero.

To illustrate Thompson's approach, let us consider the nonconservative axisymmetric Euler equations written in cylindrical coordinates:

$$Q_t + AQ_r + BQ_x + C = 0 \tag{8}$$

In the nonconservative form of the equations

$$Q = \begin{Bmatrix} \rho \\ u \\ v \\ p \end{Bmatrix} \tag{9}$$

$$A = \begin{bmatrix} v & 0 & \rho & 0 \\ 0 & v & 0 & 0 \\ 0 & 0 & v & \frac{1}{\rho} \\ 0 & 0 & \gamma p & v \end{bmatrix} \tag{10}$$

$$B = \begin{bmatrix} u & \rho & 0 & 0 \\ 0 & u & 0 & \frac{1}{\rho} \\ 0 & 0 & u & 0 \\ 0 & \gamma p & 0 & u \end{bmatrix} \tag{11}$$

$$C = \begin{Bmatrix} \frac{\rho v}{r} \\ 0 \\ 0 \\ \frac{\gamma p v}{r} \end{Bmatrix} \tag{12}$$

Thompson's procedure is illustrated using the axial boundary. The radial derivatives are grouped with the source term to rewrite Eq. (8) as

$$Q_t + BQ_x + K = 0 \tag{13}$$

Following Thompson's derivation, the matrix B is diagonalized using similarity transformation. The eigenvectors are obtained, and the left and right eigenvectors of B are calculated. The matrix S is formed, where the columns of S are the right eigenvectors r_i, and the similarity transform is defined

$$\Lambda = S^{-1}BS \tag{14}$$

Applying this transform to Eq. (13) gives

$$Q_t + SL + K = 0 \tag{15}$$

where

$$L_i = \lambda_i l_i^T Q_x \tag{16}$$

Equation (15) may be written as

$$\begin{aligned} p_t - \rho c u_t &= -L_1 - K_4 + \rho c K_2 = R_1 \\ c^2\rho_t - p_t &= -L_2 - c^2 K_1 + K_4 = R_2 \\ v_t &= -L_3 - K_2 = R_3 \\ p_t + \rho c u_t &= -L_4 - K_4 - \rho c K_2 = R_4 \end{aligned} \tag{17}$$

Solving Eq. (17) for the time derivatives, we obtain

$$\begin{aligned} \rho_t &= (1/c^2)\left[R_2 + \tfrac{1}{2}(R_1 + R_4)\right] \\ u_t &= (1/2\rho c)(R_4 - R_1) \\ v_t &= R_3 \\ p_t &= \tfrac{1}{2}(R_1 + R_4) \end{aligned} \tag{18}$$

To apply the nonreflective Thompson boundary conditions, it is necessary to determine which waves (L_1–L_4) are incoming or outgoing. For example, if the boundary in question is the downstream axial boundary, and the flow in the radial direction is outgoing and subsonic, then the L_1 wave is incoming (velocity $= U - c < 0$) and the L_2–L_4 waves are all outgoing.

At this point, the amplitude of the incoming waves are set to zero, giving the boundary condition

$$\begin{aligned} L_1 &= 0 \\ L_2 &= (u)\left(c^2\rho_x - p_x\right) \\ L_3 &= (u)(v_x) \\ L_4 &= (u + c)(P_x + \rho c u_x) \end{aligned} \tag{19}$$

and the time derivatives for the boundary points are calculated using Eq. (18).

The boundary conditions for the radial direction are obtained in a similar manner.

B. Giles' Approach

Giles[4] derived boundary conditions based on a Fourier analysis of the linearized Euler equations (LEE). Consider the unsteady part of the flow to be small disturbances, denoted by $'$, superimposed on a constant mean flow U, V. The axisymmetric LEE can be written as

$$Q'_t + AQ'_r + BQ'_x + C' = 0 \tag{20}$$

Consider the disturbance to be in the waveform

$$Q'(x,r,t) = q^R \exp i(kx + lr - \omega t) \tag{21}$$

where q^R is a constant vector. Giles' basic idea is that the dispersion relation for the preceding linear equation can be modified to prohibit the propagation of waves with group velocities directed into the computational domain. This dispersion relation is nonlinear, which implies that the boundary condition must be a nonlocal one to satisfy this condition exactly. To produce local boundary conditions, the dispersion relation is expanded in a Taylor series around the one-dimensional solution. Boundary conditions for various degrees of approximation can thus be constructed.

In the axial direction, the characteristic variables are defined as

$$\begin{aligned} r_1 &= p' - \bar{\rho}\bar{c}u' \\ r_2 &= p' - \bar{c}^2\rho' \\ r_3 &= p' + \bar{\rho}\bar{c}u' \\ r_4 &= \bar{\rho}\bar{c}v' \end{aligned} \tag{22}$$

For a subsonic outflow condition ($x = b$), the r_1 characteristic is obtained using the Giles analysis; all others are obtained from the inner solution. The second-order Giles outflow condition is

$$\frac{\partial r_1}{\partial t} = -U\left(\frac{\partial r_4}{\partial r} + \frac{r_4}{r}\right) - V\frac{\partial r_1}{\partial r} \tag{23}$$

For a subsonic inflow condition ($x = a$), the fourth-order Giles boundary condition becomes

$$\begin{aligned} \frac{\partial r_2}{\partial t} &= -V\frac{\partial r_2}{\partial r} \\ \frac{\partial r_3}{\partial t} &= -\frac{(\bar{c}-U)}{2}\left(\frac{\partial r_4}{\partial r} + \frac{r_4}{r}\right) - V\frac{\partial r_3}{\partial r} \\ \frac{\partial r_4}{\partial t} &= -V\left(\frac{\partial r_4}{\partial r} + \frac{r_4}{r}\right) - \frac{(\bar{c}+U)}{2}\frac{\partial r_3}{\partial r} - \frac{(\bar{c}-U)}{2}\frac{\partial r_1}{\partial r} \end{aligned} \tag{24}$$

This analysis is repeated to obtain the outer radial boundary condition.

C. Tam and Webb's Approach

Tam and Webb,[5] Bayliss and Turkel,[6] Hagstrom and Hariharan,[7] and Enquist and Majda[8] considered boundary conditions based on an asymptotic analysis of the linearized Euler equations with constant mean flow in the x direction.

This system of equations can be reduced to the convective wave equation for the pressure. For an outgoing wave solution at large distances, the boundary condition can be stated as

$$\frac{1}{V(\theta)}p'_t + p'_R + \frac{p'}{R} = 0 \tag{25}$$

where

$$\begin{aligned} R &= \sqrt{x^2 + r^2} \\ V(\theta) &= \bar{c}\left[\frac{x}{R}M + \sqrt{1 - \left(\frac{r}{R}M\right)^2}\right] \end{aligned} \tag{26}$$

The preceding form of the pressure boundary condition was obtained by Tam and Webb, but one can show that it is identical to the pressure condition obtained by Bayliss and Turkel and others.

However, Tam and Webb performed a rational asymptotic analysis for the full set of Euler equations. They showed that although the asymptotic pressure is only acoustic in nature, the velocity and density fluctuations contain both hydrodynamic and acoustic contributions. Using this, they arrived at a complete set of outflow boundary conditions that can be written in the following form:

$$\rho'_t = -U\rho'_x + \frac{1}{\bar{c}^2}(p'_t + Up'_x) \tag{27}$$

$$u'_t = -Uu'_x - \frac{1}{\bar{\rho}}p'_x \tag{28}$$

$$v'_t = -Uv'_x - \frac{1}{\bar{\rho}}p'_r \tag{29}$$

$$p'_t = -V(\theta)\left[\frac{x}{R}p'_x + \frac{r}{R}p'_r + \frac{p'}{R}\right] \tag{30}$$

This boundary condition is applied at the outflow boundary; at the inflow boundaries, acoustic radiation boundary conditions may be used:

$$Q'_t = -V(\theta)\left[\frac{x}{R}Q'_x + \frac{r}{R}Q'_r + \frac{Q'}{R}\right] \tag{31}$$

where Q is defined in Eq. (9).

V. Test Problem

The test problem studied was that of a monopole in a uniform flow in the axial direction. The analytic solution is

$$p'(x,r,t) = \frac{\bar{\rho}\hat{S}}{4\pi D}\left\{\left[1 + \frac{1}{\beta^2}\left(M^2 - \frac{Mx}{D}\right)\right]\omega\cos(\omega\tau) - \frac{Ux}{D^2}\sin(\omega\tau)\right\} \tag{32}$$

$$u'(x,r,t) = \frac{\hat{S}}{4\pi D}\left[\frac{1}{\beta^2\bar{c}}\left(M - \frac{x}{D}\right)\omega\cos(\omega\tau) - \frac{x}{D^2}\sin(\omega\tau)\right] \tag{33}$$

$$v'(x,r,t) = -\frac{\hat{S}r}{4\pi D^2}\left[\frac{\omega}{\bar{c}}\cos(\omega\tau) - \frac{\beta^2}{D}\sin(\omega\tau)\right] \tag{34}$$

$$\rho'(x,r,t) = \frac{p'(x,r,t)}{\bar{c}^2} \tag{35}$$

where

$$\begin{aligned} M &= \frac{U}{\bar{c}} \\ \beta &= \sqrt{1 - M^2} \\ D &= \sqrt{x^2 + (\beta r)^2} \\ \tau &= t - \frac{D - Mx}{\bar{c}\beta^2} \end{aligned} \tag{36}$$

For the described computations,

$$\begin{aligned} \omega &= \pi/2 \\ \hat{S} &= 0.01 \\ M &= 0.5 \\ \bar{\rho} = \bar{c} &= 1.0 \end{aligned} \tag{37}$$

The computational grid starts at $r = 0.5$ and ends at $r = 24.5$ in the radial direction. In the axial direction, the grid covers from $-12 < x < 12$. The grid has 300×300 points and is uniform. Again, a large number of grid points were used to reduce inaccuracies due to the interior scheme. Tests were also performed with a finer grid of 450×450 points; although the overall errors decreased, the relative performances of the boundary conditions were the same.

The point source is located at the origin. The analytic solution is specified as the initial conditions, and a Courant–Friedrichs–Lewy

(CFL) number of 0.5 is used. With no mean flow, this gives 25 points per wavelength and 191 time steps per cycle of oscillation.

For all computations, the analytic solution was specified at the inner radial boundary. The upstream axial boundary and the outer radial boundary were both treated as inflow boundaries, whereas the downstream axial boundary was treated as an outflow boundary.

VI. Implementation of Boundary Conditions

A. Thompson's Approach

The Thompson boundary condition was implemented in four ways: two were second-order accurate in time, whereas the remaining two were first-order accurate in time. The axial outflow boundary will be used to illustrate the various implementations of the Thompson boundary condition.

Because of the split operators used by the code, the implementation of the Thompson boundary conditions was greatly simplified. The axial operator used by the code is defined as

$$\frac{\partial \tilde{Q}}{\partial t} + \frac{\partial \tilde{F}}{\partial x} = 0 \tag{38}$$

Thus, Eq. (8) becomes

$$Q_t + BQ_x = 0 \tag{39}$$

since the radial derivatives and the source term do not appear in the axial operator. Using these definitions, the nonreflective outflow boundary condition becomes

$$p'_t - \bar{\rho}\bar{c}u'_t = -(U - \bar{c})(p'_x - \bar{\rho}\bar{c}u'_x) = 0 \tag{40}$$

The amplitudes of the remaining characteristic waves can thus be computed using either time or space derivatives.

At the corners, the boundary conditions for both grid faces are applied.

1. Thompson Split/Time (Th2t)

The first implementation of the Thompson boundary condition used the time derivatives to compute the amplitudes of the characteristic waves. To preserve the code's second-order time accuracy, the boundary conditions were applied at the end of both the predictor and corrector sweeps in each direction.

2. Thompson Split/Space (Th2s)

This variant used the spatial derivatives to compute the amplitude of the characteristic waves. The spatial derivatives were computed in the same manner as shown in Eqs. (6) and (7), using extrapolation when required. Note that the derivatives are computed using the primitive variables, not the conserved quantities. Again, the boundary conditions are applied at the end of the predictor and corrector sweeps in each direction.

3. Thompson/Space (Th1s)

This version also used the spatial derivatives to compute the amplitude of the characteristic waves. This time, however, the boundary conditions were only applied at the end of the appropriate operator, using fourth-order accurate one-sided differences to evaluate the spatial derivatives at the old time level. First-order accurate time derivatives are used to update the flow variables at the boundaries.

4. Thompson/Time (Th1t)

The time derivatives were used to compute the amplitude of the characteristic waves. Again, the boundary conditions were only applied at the end of the appropriate operator, using first-order accurate time derivatives.

B. Giles' Approach

Two implementations of the Giles boundary conditions were performed: the first was first-order accurate in time, whereas the second was second-order accurate in time.

1. Giles (G1)

In this version, the Giles boundary condition is implemented at the end of each time step, after both the radial and axial operators are applied. The spatial derivatives are computed using fourth-order accurate one-sided differences, with the flow variables from the old time level. The time derivatives are computed using first-order backward differences.

2. Giles Split (G2)

Next, the Giles boundary condition was split into axial and radial operators. In this formulation, the boundary conditions are applied at the end of each predictor and corrector sweep, retaining second-order accuracy in time. The spatial derivatives were calculated from the primitive variables employing the differencing method used by the inner code. Extrapolation of the primitive variables was performed when necessary.

Both Giles boundary condition formulations were unstable when applied to corner points. Since the performance of the boundary conditions at the corner points wasn't a major area of interest, the analytic solution was specified at the corner points for these calculations. To ensure that this was not causing errors of its own, a special corner treatment based on rotated one-dimensional characteristics was also tested; the performance of the Giles boundary condition was insensitive to the choice of corner treatments.

C. Tam and Webb's Approach

In their original implementation of this boundary condition, Tam and Webb used a "boundary region" of two points instead of one at each edge of the grid. No extrapolation was used in computing the spatial derivatives; this required constructing stencils that only used variables at grid points in the computational domain. This is described fully in Tam and Webb.[5] To remain consistent, the Tam and Webb boundary condition was coded using only one boundary point. For comparison, a two-point boundary region variant was also tested; the results are equivalent. Two implementations of the Tam and Webb boundary conditions were performed.

1. Tam and Webb (TW1)

In this version, the Tam and Webb boundary condition is implemented at the end of each time step, after both the radial and axial operators are applied. The spatial derivatives are computed with fourth-order accurate one-sided differences, using the flow variables from the old time level. The time derivatives are computed using first-order backward differences.

2. Tam and Webb Split (TW2)

Next, the Tam and Webb boundary condition was split into axial and radial operators. In this formulation, the boundary conditions are applied during each predictor and corrector sweep, retaining second-order accuracy in time. The spatial derivatives were calculated from the primitive variables employing the differencing method used by the inner code. Extrapolation of the primitive variables was performed when necessary.

Since the Tam and Webb outflow condition only corrects the pressure, the original code is used to compute the other flow variables. The pressure is computed using

$$p'_t = -V(\theta)\left[\frac{x}{R}p'_x\right] \tag{41}$$

for the axial sweep and

$$p'_t = -V(\theta)\left[\frac{r}{R}p'_r + \frac{p'}{R}\right] \tag{42}$$

for the radial sweep.

For the inflow conditions at the other boundaries, the radiation boundary conditions are used. These are split in a similar way.

VII. Results

Four points were chosen in the acoustic field at which to evaluate the various boundary conditions. The first point (P1) was located

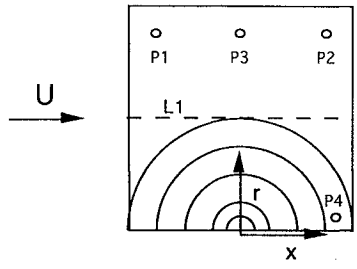

Fig. 1 Computational domain.

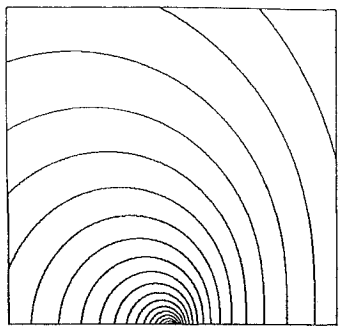

Fig. 2 Maximum pressure contours around a monopole in a uniform freestream ($M = 0.5$; analytic solution).

at $(x, r) = (-8.1, 20.5)$. The second point (P2) was at (8.1, 20.5). These points illustrate the effect of the boundary conditions on the corners of the flowfield, where the waves are not aligned with the boundaries. The third point (P3) was located at (0, 20.5). With no mean flow, this point shows the effectiveness of the radial boundary conditions when the wave velocity is normal to the boundary. The fourth point (P4) was located at (10.4, 2). With no mean flow, this point shows the effectiveness of the axial boundary conditions when the outgoing wave velocity is normal to the boundary. Also, an axial line (L1) was defined at $r = 12.5$ to better illustrate the effect of implementation differences on the performance of the various boundary conditions. Figure 1 shows the location of these points and lines in the flowfield.

At each point, the maximum amplitude of the pressure during each cycle was computed and compared with the analytic solution. The relative pressure error was used to compare the results. It is defined as

$$(\text{Error})_{\text{cycle}} = \left(\frac{|P_{\max}|_{\text{computed}} - |P_{\max}|_{\text{analytic}}}{|P_{\max}|_{\text{analytic}}} \right)_{\text{cycle}} \tag{43}$$

where $|P_{\max}|_{\text{analytic}}$ is the maximum amplitude of the wave given in Eq. (32).

Again, the inner radial boundary for all computations was specified directly from the analytic solution.

A. Monopole in a Uniform Freestream ($M = 0.5$)

Figure 2 shows the maximum pressure contours for the exact solution.

1. Thompson

All three implementations were all nearly equivalent. The two second-order versions (Th2s and Th2t) returned identical results, whereas the stable first-order implementation (Th1s) was virtually indistinguishable. Figure 3 shows the maximum pressure contours for the Th2t implementation. Figure 4 shows the results on the L1 line from the three implementations. Figure 5 shows the results of the Th2t implementation at the four test points.

The Thompson inflow condition did not perform well. For all three versions, relative pressure errors of 70% were computed at P1. It was theorized that the low performance of the inflow boundary condition in this case was due to the errors caused by the outgoing acoustic wave velocities not being normal to the boundary.

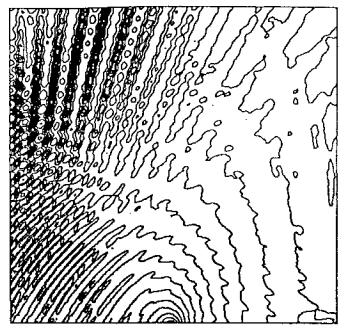

Fig. 3 Maximum pressure contours around a monopole in a uniform freestream ($M = 0.5$; Thompson boundary condition).

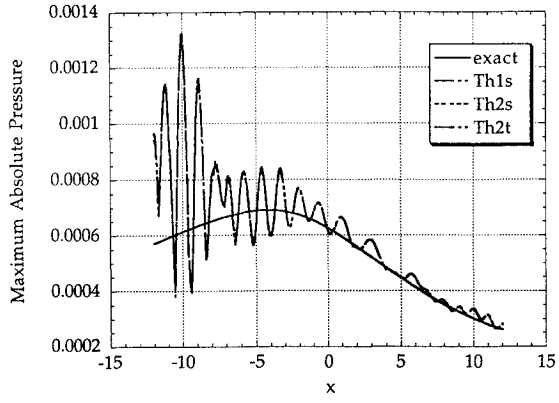

Fig. 4 Effect of implementation on the maximum pressure for a uniform flow about a monopole ($M = 0.5$; Thompson boundary condition).

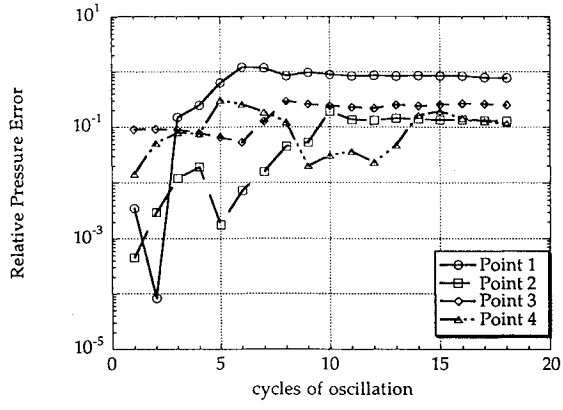

Fig. 5 Effect of implementation on the relative pressure error at test points for a uniform flow about a monopole ($M = 0.5$; Thompson boundary condition).

The outflow condition performed much better; at P2, the relative pressure errors were below 20%. Here, the wave velocities are nearly normal to the boundary.

The inflow condition specified at the outer radial boundary (P3) resulted in relative pressure errors of 20–30%.

The Thompson boundary condition performed best at P4; the velocity of the outgoing waves were nearly normal to the boundary, and the proximity of the fully specified boundary kept numerical noise to a minimum.

In general, the Thompson boundary condition was the least accurate of the boundary conditions tested.

2. Giles

Although the differences in the results were minor, the second-order Giles implementation (G2) slightly outperformed the first-order (G1) version. Figure 6 shows the L1 results from the two implementations. Figure 7 shows the results of the G2 run at the four test points. Figure 8 shows the maximum pressure contours for the G2 run.

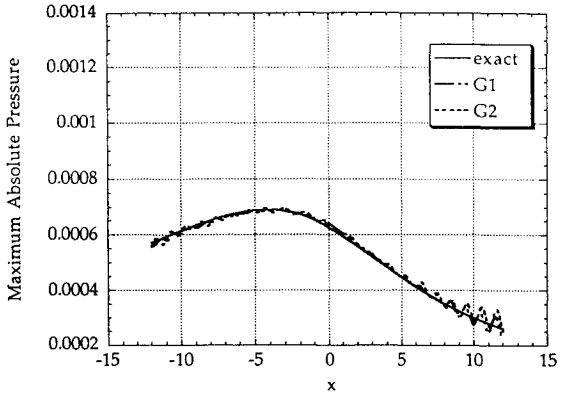

Fig. 6 Effect of implementation on the maximum pressure for a uniform flow about a monopole (M = 0.5; Giles boundary condition).

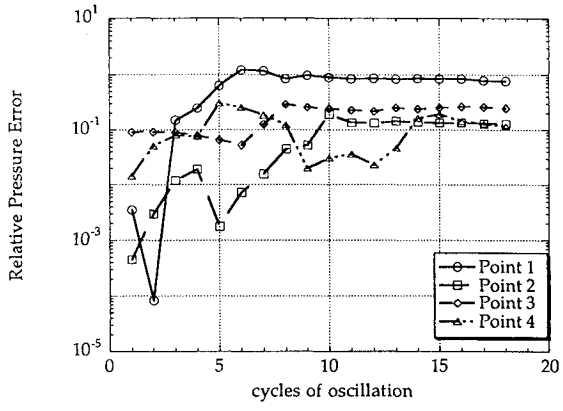

Fig. 7 Effect of implementation on the relative pressure error at test points for a uniform flow about a monopole (M = 0.5; Giles boundary condition).

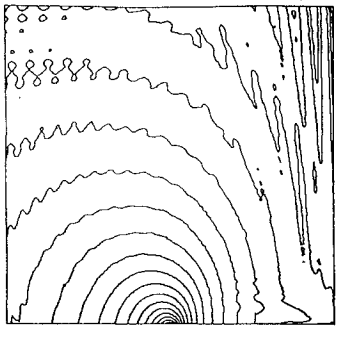

Fig. 8 Maximum pressure contours around a monopole in a uniform freestream (M = 0.5; Giles boundary condition).

The Giles inflow condition worked very well, with relative pressure errors below 3% at P1 and P3. At P4, the proximity of the fully specified boundary kept the relative pressure errors below 5%.

The Giles outflow condition did not perform as well as the inflow condition, with the error at P2 nearly reaching 20%.

The Giles boundary condition is the second best of the three formulations tested.

3. Tam and Webb

Figure 9 shows the results of the runs using the Tam and Webb boundary conditions; again, the second-order implementation (TW2) was slightly better than the first-order implementation (TW1). Figure 10 shows the results of the TW2 run at the four test points. Figure 11 shows the maximum pressure contours for the TW2 run.

Radiation inflow conditions were used at the upstream axial and outer radial boundaries; these resulted in errors of 5% at P1 and 3% at P3.

The Tam and Webb outflow condition performed very well, giving errors of 1% at P2 and P4.

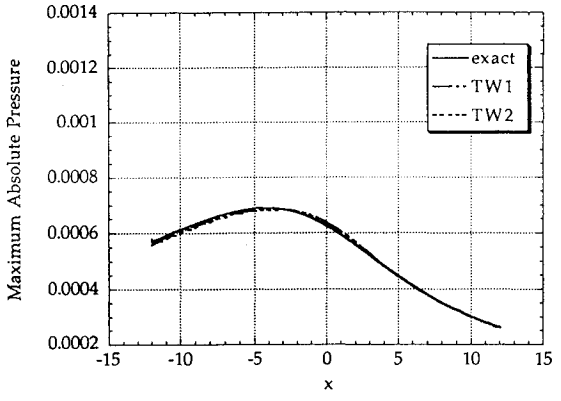

Fig. 9 Effect of implementation on the maximum pressure for a uniform flow about a monopole (M= 0.5; Tam and Webb boundary condition).

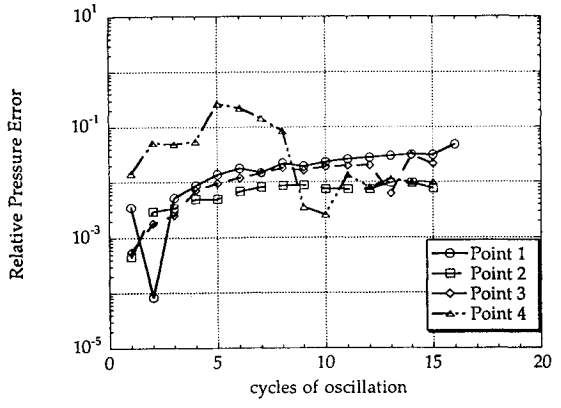

Fig. 10 Effect of implementation on the relative pressure error at test points for a uniform flow about a monopole (M= 0.5; Tam and Webb boundary condition).

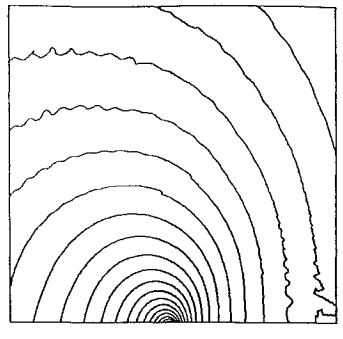

Fig. 11 Maximum pressure contours around a monopole in a uniform freestream (M = 0.5; Tam and Webb boundary condition).

The Tam and Webb outflow boundary is the best of the formulations tested, resulting in lower errors than the exact boundary conditions. The only drawback to this formulation is its present restriction to uniform mean flows.

VIII. Conclusions

Several boundary conditions for computational aeroacoustics were evaluated, namely, Giles,[4] Tam and Webb,[5] and Thompson.[2,3] The same discretization scheme was used to compute sound radiation from a monopole placed in a moving stream, but with the boundary treatment as described by one of the aforementioned approaches. For each boundary condition, various implementations were tested to study sensitivity of their performance to the implementation procedure. In general, slight improvement in the performance of each scheme can be achieved via the implementation procedure.

With the best achieved performance for each boundary treatment, the following conclusions can be drawn regarding their comparative performance:

1) For outflow boundary treatment, the only acceptable performance was that of Tam and Webb. The performance of the other schemes might be acceptable only in special cases wherein the flow is nearly one dimensional, perpendicular to the boundary. But even under such conditions, their performance did not surpass that of Tam and Webb. However, it should again be noted that the Tam and Webb boundary condition is developed for the case of a uniform mean flow only.

2) For inflow boundary treatment, the Giles boundary condition was acceptable, as well as the radiation boundary condition of Tam and Webb applied to inflow treatment. Again, it should be noted that the radiation boundary condition is formulated for the case of a uniform mean flow only. The Thompson inflow boundary treatment resulted in considerable reflection near the inflow boundary.

References

[1]Mankbadi, R. R., Hayder, M. E. and Povinelli, L. A., "Structure of Supersonic Jet Flow and Its Radiated Sound," *AIAA Journal*, Vol. 32, No. 5, 1994, pp. 897–906.

[2]Thompson, K. W., "Time-Dependent Boundary Conditions for Hyperbolic Systems," *Journal of Computational Physics*, Vol. 68, Jan. 1987, pp. 1–24.

[3]Thompson, K. W., "Time-Dependent Boundary Conditions for Hyperbolic Systems II," *Journal of Computational Physics*, Vol. 89, Aug. 1990, pp. 439–461.

[4]Giles, M. B., "Nonreflecting Boundary Conditions for Euler Equation Calculations," *AIAA Journal*, Vol. 28, No. 12, 1990, pp. 2050–2058.

[5]Tam, C. K. W., and Webb, J. C., "Dispersion-Relation-Preserving Finite Difference Schemes for Computational Acoustics," *Journal of Computational Physics*, Vol. 107, Aug. 1993, pp. 262–281.

[6]Bayliss, A., and Turkel, E., "Far Field Boundary Conditions for Compressible Flows," *Journal of Computational Physics*, Vol. 48, Nov. 1982, pp. 182–199.

[7]Hariharan, S. I., and Hagstrom, T., "Far Field Expansion for Anisotropic Wave Equations," *Proceedings of the Second IMACS Symposium on Computational Acoustics*, edited by D. Lee, A. Cakmak, and R. Vichnevetsky, North-Holland, 1990, pp. 283–294.

[8]Enquist, B., and Majda, A., "Radiation Boundary Conditions for Acoustic and Elastic Wave Calculations," *Communications on Pure and Applied Mathematics*, Vol. 32, No. 3, 1979, pp. 313–357.

[9]Gottlieb, D., and Turkel, E., "Dissipative Two-Four Method for Time Dependent Problems," *Mathematics of Computation*, Vol. 30, No. 136, 1976, pp. 703–723.

[10]Farouk, B., Oran, E. S., and Kailasanath, K., "Numerical Simulations of the Structure of Supersonic Shear Layers," *Physics of Fluids A*, Vol. 3, No. 11, 1991, pp. 2786–2798.

[11]Ragab, S. A., and Sheen, S., "The Nonlinear Development of Supersonic Instability Waves in a Mixing Layer," *Physics of Fluids A*, Vol. 4, No. 3, 1991, pp. 553–566.

[12]Sankar, L. N., Reddy, N. N., and Hariharan, N., "A Comparative Study of Numerical Schemes for Aero-Acoustic Applications," *Computational Aero- and Hydro-Acoustics*, FED-Vol. 147, American Society of Mechanical Engineers, Fairfield, NJ, 1993, pp. 35–40.